Biomedicine & Pharmacotherapy 138 (2021) 111483

Contents lists available at ScienceDirect

Biomedicine & Pharmacotherapy

journal homepage: www.elsevier.com/locate/biopha

Original article

Oxidative stress cytotoxicity induced by platinum-doped magnesia nanoparticles in cancer cells☆

Mohamed Qasim Al-Fahdawi [a], Faris A.J. Al-Doghachi [b], Qasim Khlaif Abdullah [c], Ruaa Tareq Hammad [d], Abdullah Rasedee [e,*], Wisam Nabeel Ibrahim [f,g,**], Hussah Abdullah Alshwyeh [h], Areej A Alosaimi [h], Sahar Khamees Aldosary [h], Eltayeb E. M. Eid [i,***], Rozita Rosli [a], Y.H. Taufiq-Yap [j,k], Nagi A. Al-Haj [a,l], Mothanna Sadiq Al-Qubaisi [a]

[a] Institute of Bioscience, Universiti Putra Malaysia, 43400 UPM Serdang, Selangor, Malaysia
[b] Department of Chemistry, Faculty of Science, University of Basra 61004, Basra, Iraq
[c] DCH/Pediatric Department, Ramadi Teaching Hospital for Gynecology and Childhood, University of Anbar, Ramadi, Iraq
[d] Department of Chemistry, Faculty of Science; University of Anbar, Ramadi, Iraq
[e] Department of Veterinary Laboratory Diagnosis, Faculty of Veterinary Medicine, Universiti Putra Malaysia, 43400 UPM Serdang, Selangor, Malaysia
[f] Department of Biomedical Science, College of Health Sciences, QU health, Qatar University, Doha, Qatar
[g] Biomedical and Pharmaceutical Research Unit, QU health, Qatar University, Doha, Qatar
[h] Department of Biology, College of Science, Imam Abdulrahman Bin Faisal University (IAU), Dammam 31441-1982, Saudi Arabia
[i] Department of Pharmaceutical Chemistry and Pharmacognosy, Unaizah College of Pharmacy, Qassim University, Saudi Arabia
[j] Catalysis Science and Technology Research Centre, Faculty of Science; Universiti Putra Malaysia, 43400 UPM Serdang, Selangor, Malaysia
[k] Faculty of Science and Natural Resources, Universiti Malaysia Sabah, 88300 Kota Kinabalu, Sabah, Malaysia
[l] Faculty of Medicine and Health Sciences, Sana'a University, Yemen

ARTICLE INFO

Keywords:
Pt/MgO nanoparticles
Cytotoxicity
Oxidative stress
Lipid peroxidation
Apoptosis
Lung cancer
Colonic cancer

ABSTRACT

The aim of this study was to prepare, characterize, and determine the in vitro anticancer effects of platinum-doped magnesia (Pt/MgO) nanoparticles. The chemical compositions, functional groups, and size of nanoparticles were determined using X-ray diffraction, Fourier transform infrared spectroscopy, energy dispersive X-ray spectroscopy, transmission electron microscopy, and scanning electron microscopy. Pt/MgO nanoparticles were cuboid and in the nanosize range of 30–50 nm. The cytotoxicity of Pt/MgO nanoparticles was determined via the 3-(4,5-dimethylthiazol-2-yl)−2,5-diphenyltetrazolium bromide assay on the human lung and colonic cancer cells (A549 and HT29 respectively) and normal human lung and colonic fibroblasts cells (MRC-5 and CCD-18Co repectively). The Pt/MgO nanoparticles were relatively innocuous to normal cells. Pt/MgO nanoparticles downregulated Bcl-2 and upregulated Bax and p53 tumor suppressor proteins in the cancer cells. Pt/MgO nanoparticles also induced production of reactive oxygen species, decreased cellular glutathione level, and increased lipid peroxidation. Thus, the anticancer effects of Pt/MgO nanoparticles were attributed to the induction of oxidative stress and apoptosis. The study showed the potential of Pt/MgO nanoparticles as an anticancer compound.

1. Introduction

Metal-containing drugs can modify cellular reactions through the production of reactive oxygen species (ROS) [1,2]. Metallic elements have unique biological properties that are attributed to their ability to easily lose electrons and produce soluble cations in biological fluids

☆ The authors have no relevant affiliations or financial involvement with any organization or entity with a financial interest in or financial conflict with the subject matter or materials discussed in the manuscript. This includes employment, consultancies, honoraria, stock ownership or options, expert testimony, grants or patents received or pending, or royalties.

* Corresponding author.
** Corresponding author at: Department of Biomedical Science, College of Health Sciences, QU health, Qatar University, Doha, Qatar.
*** Corresponding author.
E-mail addresses: rasedee@upm.edu.my (A. Rasedee), w.ibrahim@qu.edu.qa (W.N. Ibrahim), eem.eid@qu.edu.sa (E.E.M. Eid).

https://doi.org/10.1016/j.biopha.2021.111483
Received 28 January 2020; Received in revised form 20 February 2021; Accepted 4 March 2021

while serving as charged vehicles in cellular and body mechanisms [3–6]. These metallic elements may combine with biological molecules e.g. nucleic acids and proteins [7,8] for the maintenance of homeostasis. Positively charged metal ions can also facilitate catalysis through the control of electron flow in enzymes and substrates [9–13].

Transition metals such as silver and platinum were shown to promote production of oxidative radicals and lipid peroxidation [13–16] that may cause oxidation-related damage to unsaturated fatty acids [17,18], decreasing membrane fluidity and eventually causing cell death [19, 20]. For the transition metals to be effective and efficacious therapeutic compounds, the oxidative radicals generated by the treated cells should selectively destroy diseased and not normal cells.

Metallic nanoparticles are emerging as promising diagnostic and anticancer compounds. These nanoparticles can provide better targeting, delivery, tumor deposition, and gene silencing characteristics than conventional anticancer compounds [21].

We previously showed that the metal nanoparticles, NiZn ferrite, are toxic to cancer cells through the induction of oxidative stress [1]. Currently, there is little information on the role of platinum-containing nanoparticles as an anti-cancer agent. Thus, the hypothesis of this study is that platinum-doped magnesia (Pt/MgO) nanoparticles inhibit lung and colon cancer cell proliferation through the induction of oxidative stress and apoptosis. In this study, we determined the structural and morphological characteristics and effect of Pt/MgO nanoparticles on the human colon (HT29) and lung (A549) cancer cell lines. To our knowledge, this is a first report on the in vitro anti-cancer effect of Pt/MgO nanoparticles.

2. Materials and methods

2.1. Chemicals and reagents

Trypsin/ethylenediaminetetra acetic acid (EDTA) solution was purchased from Invitrogen (Carlsbad CA, USA). Dimethylsulfoxide (DMSO), phosphate-buffered saline (PBS), 3-(4,5-dimethylthiazol-2-yl)−2,5-diphenyltetrazolium bromide (MTT), Dulbecco's modified Eagle's medium (DMEM), diphenylamine (DPA) reagent (100 mL glacial acetic acid 1.5 g diphenylamine, 1.5 mL concentrated sulfuric acid 0.5 mL and 16 mg/mL acetaldehyde stock), trypan blue dye, and N-acetyl-L-cysteine (NAC) were purchased from Sigma Chemical Company (Perth Western, Australia).

2.2. Preparation of Pt/MgO nanoparticles

The Pt/MgO nanoparticles were prepared using the precipitation method. MgO was prepared using 0.1 M aqueous solution of Mg $(NO_3)_2.6H_2O$ (Merck; >99.0%) and 1 M K_2CO_3 (Merck; >99.7%) as precipitant. The precipitate (sample) was filtered and washed with hot water and dried at 120 °C for 12 h. Subsequently, the dried sample was pre-calcined in air at 500 °C for 5 h to remove CO_2. The sample was then pressed into a disc at 600 kg/m^2 (Hydrolic for KBr disc) and calcined at 1150 °C for 20 h to enhance its mechanical properties.

The sample was impregnated with 5% Pt using $Pt(C_5H_7O_2)_2{\cdot}H_2O$ (Acros Chemicals; >99%), dissolved with dichloromethane, for 5 h to produce $Pt(acac)_2$/MgO. After impregnation, the samples were dried at 120 °C for 12 h. The dried samples were crushed and sieved (250 μm) to obtain particles of 80–150 or 150–250 μm in diameter. Finally, the Pt^{2+} phase nanoparticles were reduced to metal Pt^o phase at the active site of the nanoparticles, using 5% H_2/Ar, to produce Pt/MgO.

2.3. Physicochemical properties of nanoparticles

2.3.1. Scanning electron microscopy and energy dispersive X-ray spectroscopy

Scanning electron microscopy (SEM) [Model LEO 1450VP (LEO Electron Microscopy Ltd Cambridge, UK)], with an accelerating voltage of 30 kV and energy dispersive X-ray spectroscopy (EDX) were used to determine the morphology and elemental composition of powdered nanoparticles, respectively. The samples were degassed in an evacuated heated chamber at 100 °C overnight. Prior to SEM scanning, dried samples were spread over double-sided conductive tape and adhered to the specimen stub.

2.3.2. Transmission electron microscopy

Transmission electron microscopy (TEM) (Hitachi H-7100, Japan) was used to determine the fine structure of the crystals. The nanoparticle powder was disseminated in deionized water, placed on carbon-cover copper grids on filter paper and dried at room temperature before viewing.

2.3.3. X-ray diffraction

X-ray diffraction (XRD)characterization of nanoparticle powder was performed using the Shimadzu diffractometer model XRD 6000(Japan). The analysis employed Cu-K_α radiation generated by a Philips glass diffraction X-ray tube broad focus 2.7 kW type at ambient temperature. The crystallite size D of the samples was calculated by the Debye-Scherrer's relationship according to standard procedures [1,2] using the following formula:

$$D = 0.9\,\lambda / (\beta \cos\theta)$$

where D is the crystallite size, λ is the incident X-ray wavelength, β is the full-width at half-maximum, and θ is the diffraction angle.

2.3.4. Fourier transform infrared

Fourier transform infrared FTIR spectra for powdered nanoparticles were recorded over the range of 400–4000 cm^{-1} on a Thermo Nicolet Nexus, Smart Orbit spectrometer (Shelton, USA) using 1% in 200 mg spectroscopic-grade potassium bromide (KBr) under 10 tons of pressure.

2.3.5. Thermogravimetric analysis

The thermal strength of the nanoparticles was investigated using the Mettler Toledo TG-SDTA apparatus (Pt crucibles, Pt/Pt– Rh thermocouple) (Switzerland), with a purge gas (nitrogen) flow rate of 30 mL min^{-1} and heating rate of 10 °C min^{-1}, from room temperature to 1000 °C.

2.3.6. Brunauer, Emmett and Teller analysis

The total surface area of the nanoparticles was determined at −196 °C using the nitrogen adsorption-desorption analyzer (Surfer analyzer, Milan, Italy).

2.3.7. Hydrodynamic size and zeta potential

The hydrodynamic size and zeta potential of the Pt/MgO nanoparticle suspension (1 μg nanoparticles dispersed in 1 mL of ultra-deionized water) were determined using the ZetaSizer Nano ZS (Malvern Instruments Ltd Malvern, UK) with dynamic light scattering.

2.3.8. Cell culture

Four virus-negative cell lines; human colorectal adenocarcinoma (HT29, passage number 20–25), human lung carcinoma (A549, passage number 25–30), normal human colon (CCD-18Co, passage number 20–24), and normal human lung (MRC-5, passage number18–23) cells, were purchased from the American Type Culture Collection (ATCC; Rockville, MD, USA). The cells in DMEM (Sigma Aldrich, USA) supplemented with 10% FBS and 1% penicillin (100 U/mL) (Isocillin, Aventis, Germany) were cultured in an incubator at 37 °C under 5% CO_2.

2.3.9. 3-(4,5-dimethylthiazol-2-yl)−2,5-diphenyltetrazolium bromide assay

The Pt/MgO nanoparticles were mixed with DMEM medium (Sigma Aldrich, USA) containing 10% heat-inactivated FBS and a nanoparticle

colloidal suspension obtained using the ultrasound method [1,2]. 200 μL of 5×10^3 cells/mL cell suspension were added to each well of a 96-well culture plate to a final concentration 1×10^3 cells/well. After 24 h, the medium was aspirated and replaced with 200 μL fresh medium containing nanoparticles at concentrations ranging from 1.56 to 100 μg/mL, and chemotherapeutic agents (oxaliplatin for HT29 and CCD-18Co cells, and paclitaxel for A549 and MRC-5 cell) at 0.156–10.0 μg/mL. The last row was used for non-treatment control. The plates were then incubated at 37 °C under 5% CO_2, for 24 h.

The medium was aspirated, and the cells washed with PBS buffer thrice to remove test compounds, and replaced with fresh medium. Then, 200 μL of 5 mg/mL 3-(4,5-dimethylthiazol-2-yl)−2,5-diphenyltetrazolium bromide (MTT) solution were added to each well and the plate incubated at 37 °C under 5% CO2for 4–6 h. The MTT-containing medium was then carefully removed and200 μL DMSO added to each well to dissolve the formazan crystals. The plates were read on automated spectrophotometric EL 340 multiplate reader (Bio-Tek Instruments Inc., USA) at 570 nm. The viability was determined using the following formula:

$$\text{Viability}(\%) = \frac{\text{OD}_{\text{treated}}}{\text{OD}_{\text{nontreated}}} \times 100$$

Where OD is the optical density.

The 24 h IC_{50} (50% cell growth inhibition concentration) values of Pt/MgO nanoparticles on cancer cells were determined from the concentration-response curve for each test compound and cell line.

2.3.10. Caspases

The effects of treatment on caspase-3 (with or without pretreatment with 3 mM NAC), -8 and -9 activities were determined using commercial colorimetric assay kits (Promega, Madison, WI, USA) in accordance to the recommended protocol.

2.3.11. Quantification of Bax, p53, Bcl-2 and cytochrome C protein assay

The levels of p53, Bax, Bcl-2, and cytochrome C proteins in cells treated with Pt/MgO nanoparticles were determined using ELISA assay kits (Abcam, Cambridge, MA, USA).

2.3.12. Microscopic examination of cell morphology

200 μL of cell suspensions seeded in a 6-well plate, to contain 1×10^4 cells/well, were treated with the IC_{50} concentration of Pt/MgO nanoparticles. The morphology of the cells was examined under inverted light microscopy.

2.3.13. Lipid peroxidation, reactive oxygen species, glutathione and mitochondrial transmembrane potential

The levels of lipid peroxidation and concentrations of reactive oxygen species and glutathione in normal and cancer cells were determined by malondialdehyde (MDA) and dichlorofluorescein synthesis and Ellman method, respectively. 200 μL of 2×10^4 cells/mL cell suspension in DMEM were seeded in each well of 6-well tissue culture plates. After incubation for 24 h to allow for cell attachment, the cells were subjected to treatment with 12.5 μg/mL Pt/MgO nanoparticle samples. The plates were then incubated at 37 °C under 5% CO2 for 24 h. The medium was aspirated, and the plates washed with cold phosphate-buffered saline to remove dead cells.

The effect of nanoparticles on the mitochondrial membrane potential (MMP) was determined by the rhodamine 123 efflux method. 3 μL of 5 mg/mL rhodamine solution were incubated with 0.5 mL of 1×10^6/mL cell suspension in phosphate-buffered saline. The rhodamine 123 efflux or retention was analyzed using FACSCalibur™ flow cytometry (Becton Dickinson, NJ, USA) and the data were analyzed using CellQuest 3.3 software (Becton Dickinson). The assays were done as previously described [1].

2.3.14. Statistical analysis

All experiments were done in triplicates unless otherwise indicated. The data were expressed as means ± standard deviation. All statistical analyses were performed using the Minitab statistical software (Minitab Inc., State College, PA). The significance of treatment effects was determined using one-way analysis of variance (ANOVA) followed by Dunnett's comparison tests. Significance among means was determined at $p < 0.05$.

3. Results

3.1. Characterization

3.1.1. Morphological and elemental analysis of nanoparticles

3.1.1.1. Scanning electron microscopy and energy dispersive X-ray spectroscopy. The SEM and EDX micrographs for the pure Pt/MgO nanoparticle samples are shown in Figs. 1A and 2, respectively. The Pt/MgO nanoparticles formed large clusters, indicating presence of strong interactions that caused the nanoparticles to aggregate. The sample homogeneity and overall physical properties of Pt/MgO nanoparticles can be improved by adding an appropriate agent or with the use of physical techniques, such as sonication and stirring [1,2].

3.1.1.2. Transmission electron microscopy. The ultrastructure of pure Pt/MgO nanoparticles was viewed under TEM (Fig. 1B). It is apparent that the Pt/MgO nanoparticles are cuboid in shape with diameters ranging from 30 to 50 nm. Most of the Pt/MgO nanoparticles were aggregated. This phenomenon suggests that there are strong interactions amongst nanoparticles, thus, confirming the findings from SEM analysis.

3.1.2. Crystallinity

Fig. 1C depicting the X-ray diffraction patterns shows that the Pt/MgO nanoparticles comprise of the cuboid magnesia phase at $2\theta = 37.1°$ (1 1 1), 42.9° (2 0 0), 62.2° (2 2 0), 74.7° (3 1 1), and 78.9° (2 2 2) (JSPDS file No: 00–002–1207) [22]. The diffraction peaks recorded at $2\theta = 39.8$ (1 1 1), 46.4 (2 0 0), and 67.7 (2 2 0) are manifestations of the cuboid form of Pt. The complexation with magnesium oxide nanoparticles, in fact, improved the stability of the cuboid Pt and produced high Brunauer–Emmett–Teller (BET) surface areas. The size of the Pt/MgO crystals determined by the Debye-Scherrer's equation was 38 nm. The BET specific surface area (S_{BET}), pore volume, and pore radius of the Pt/MgO nanoparticles were 10.46 m^2/g, 0.41 cm^3/g, and 18.26°A, respectively. The calculated pore volume to S_{BET} ratio was 48.4 10^{-9} m.

3.1.3. Infrared absorption bands

The vibrational band at 3484 cm^{-1} indicates that there is moisture in the Pt/MgO nanoparticle samples (Fig. 1D). The peaks at approximately at 3135, 1636 and 1528 crn^{-1} represent the stretching and bending modes of hydroxyl groups. Although the samples were subjected to high temperature calcination, these modes show that the Brönsted acid-active sites are present on the surface of Pt/MgO nanoparticles. The band at 3746 cm^{-1} corresponds to -OH stretching vibration bonded with Mg and bending bond at 1447 cm^{-1}. The intensity of the peak at 3746 cm^{-1} for MgO nanoparticles with adsorbed Pt was greater than for pure MgO nanoparticles [23].

3.1.4. Thermogravimetric analysis

Thermogravimetric analysis was used to investigate the behaviour of samples subjected to heating to induce sintering. The thermogravimetric curve for pure Pt/MgO nanoparticles and mass loss as determined from thermogravimetric analysis are consistent with the decomposition of calcined Pt/MgO nanoparticles (Fig. 1E). Thus, calcination of Pt/MgO nanoparticles at a temperature range of 25–400 °C caused the

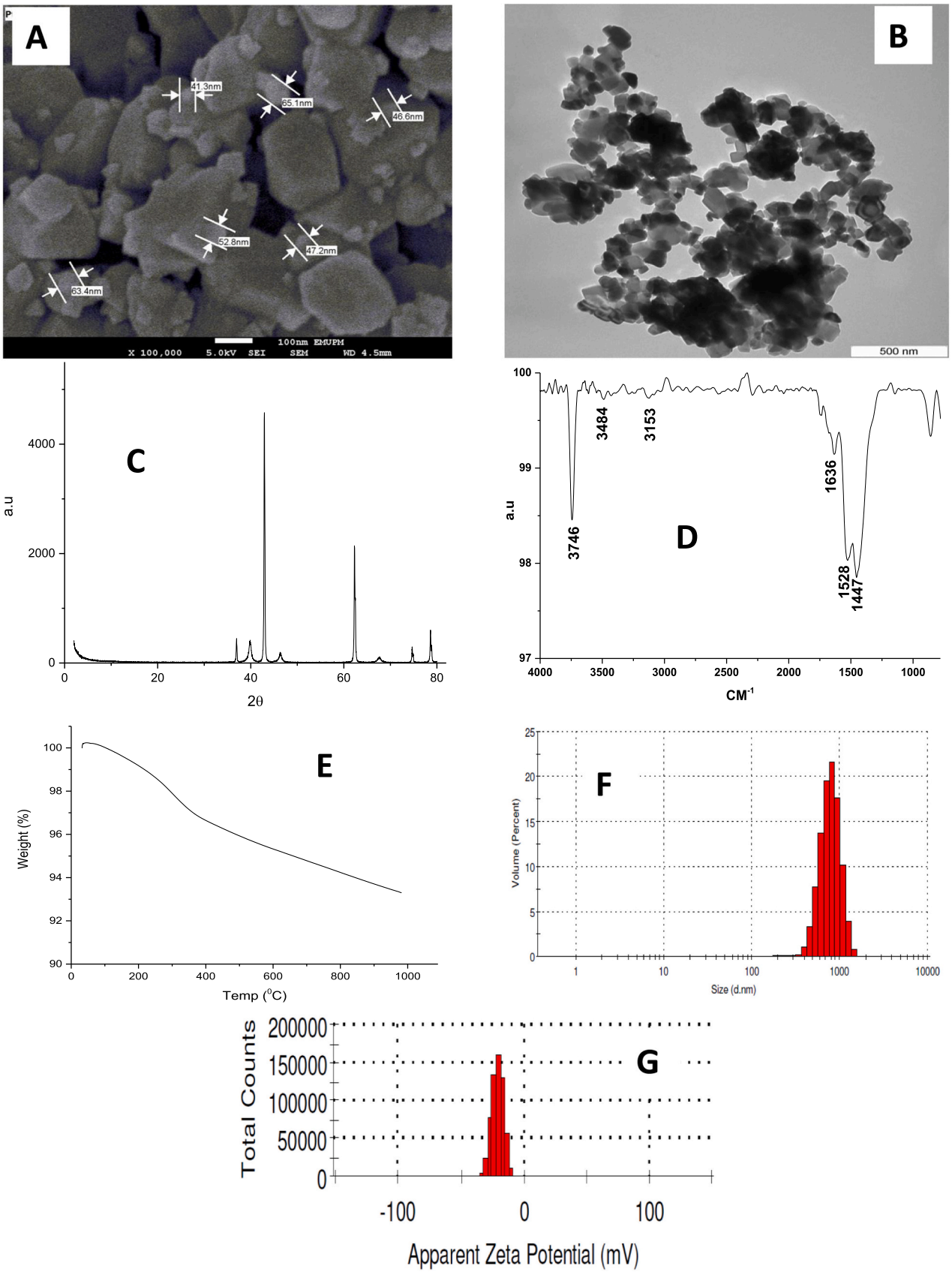

Fig. 1. Characterization of Pt/MgO nanoparticles by: (A) scanning electron micrograph, (B) transmission electron micrograph, (C) X-ray diffraction pattern, (D) Fourier transform infrared spectrum, (E) thermograph showing phase with thermal treatments. (F) hydrodynamic size, and (G) zeta potential showing negative surface charge.

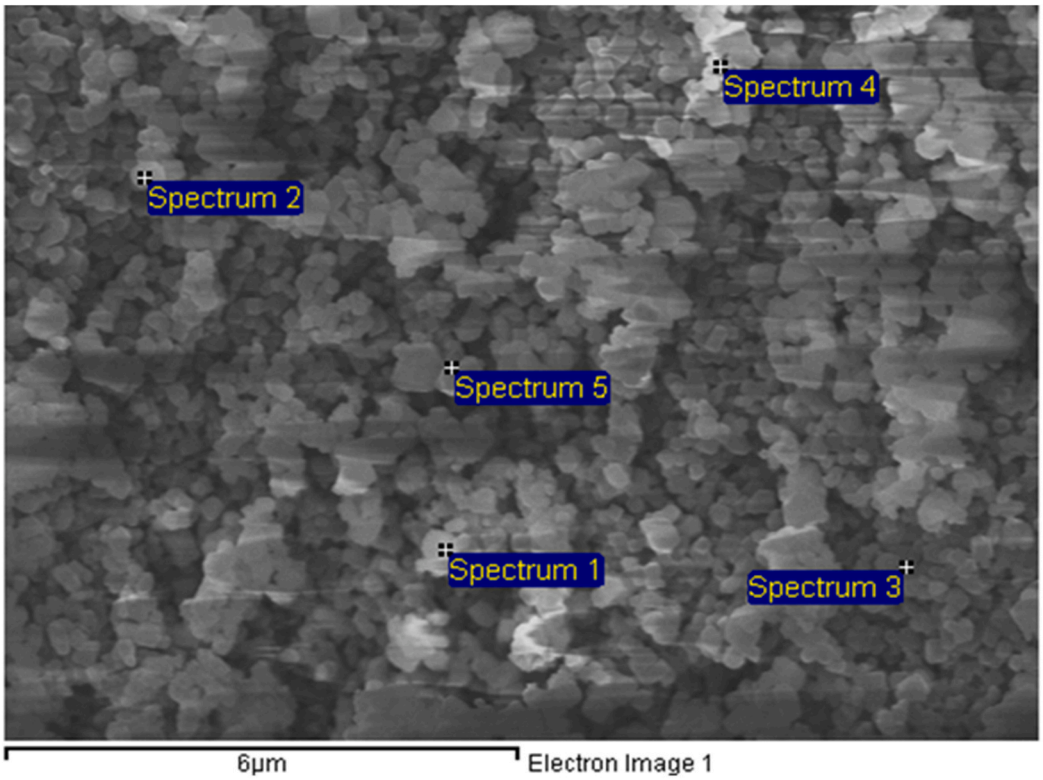

Pt-NP	Instats.	C	O	Mg	Pt	Total
Spectrum 1	Yes	14.02	46.90	35.98	3.10	100.00
Spectrum 2	Yes	12.82	47.51	39.15	0.51	100.00
Spectrum 3	Yes	13.09	36.35	50.55	0.00	100.00
Spectrum 4	Yes	11.48	49.34	39.18	0.00	100.00
Spectrum 5	Yes	12.73	42.54	42.81	1.92	100.00
Mean		12.83	44.53	41.53	1.11	100.00

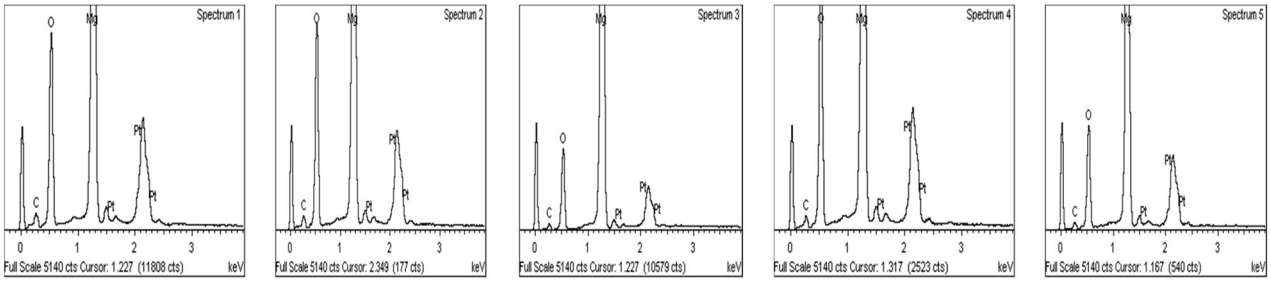

Fig. 2. Energy dispersive X-ray spectroscopy of pure Pt/MgO nanoparticles.

elimination of physically adsorbed water. The second mass loss began at approximately 400 °C and ended at 1000 °C and this is ascribed to the degradation of carbon residue to form CO_2 gas.

3.1.5. Hydrodynamic size and zeta potential

The average hydrodynamic diameter, polydispersity index (PDI), and zeta potential for the Pt/MgO nanoparticle suspensions were 932.3 ± 22.0 nm, 0.598 ± 0.0951, and −20.7 ± 4.3 mV, respectively (Fig. 1F and G).

3.2. Anticancer of Pt/MgO nanoparticles

3.2.1. Cytotoxicity

The Pt/MgO nanoparticles showed significant ($p < 0.05$) toxic effects towards the A549 cells at all concentrations used in this study. In the case of HT29 cells, the lowest Pt/MgO nanoparticles concentration of 1.56 μg/mL had no significant effect ($p > 0.05$) on cell growth. However, the Pt/MgO nanoparticle at the same concentration caused 20% growth inhibition of the A549 cells (Fig. 3). The IC_{50} values of Pt/MgO nanoparticles calculated from the dose-response curves are shown in Table 1. The MTT assay showed that the viability of HT29 cells decreased significantly ($p < 0.05$) after treatment with 6.125 and 12.5 μg/mL Pt/MgO nanoparticles for 24 h (Fig. 3). On the other hand, the CCD-18Co cells were least sensitive to Pt/MgO nanoparticles among cells used in this study, with IC_{50} of 48 μg/mL, while the HT29 cells were most sensitive with IC_{50} of 13.7 μg/mL. The IC_{50} value of Pt/MgO nanoparticles for the MRC-5 cells were more than 12 times higher than that for the A549 cells. Furthermore, lung cancer cells were more

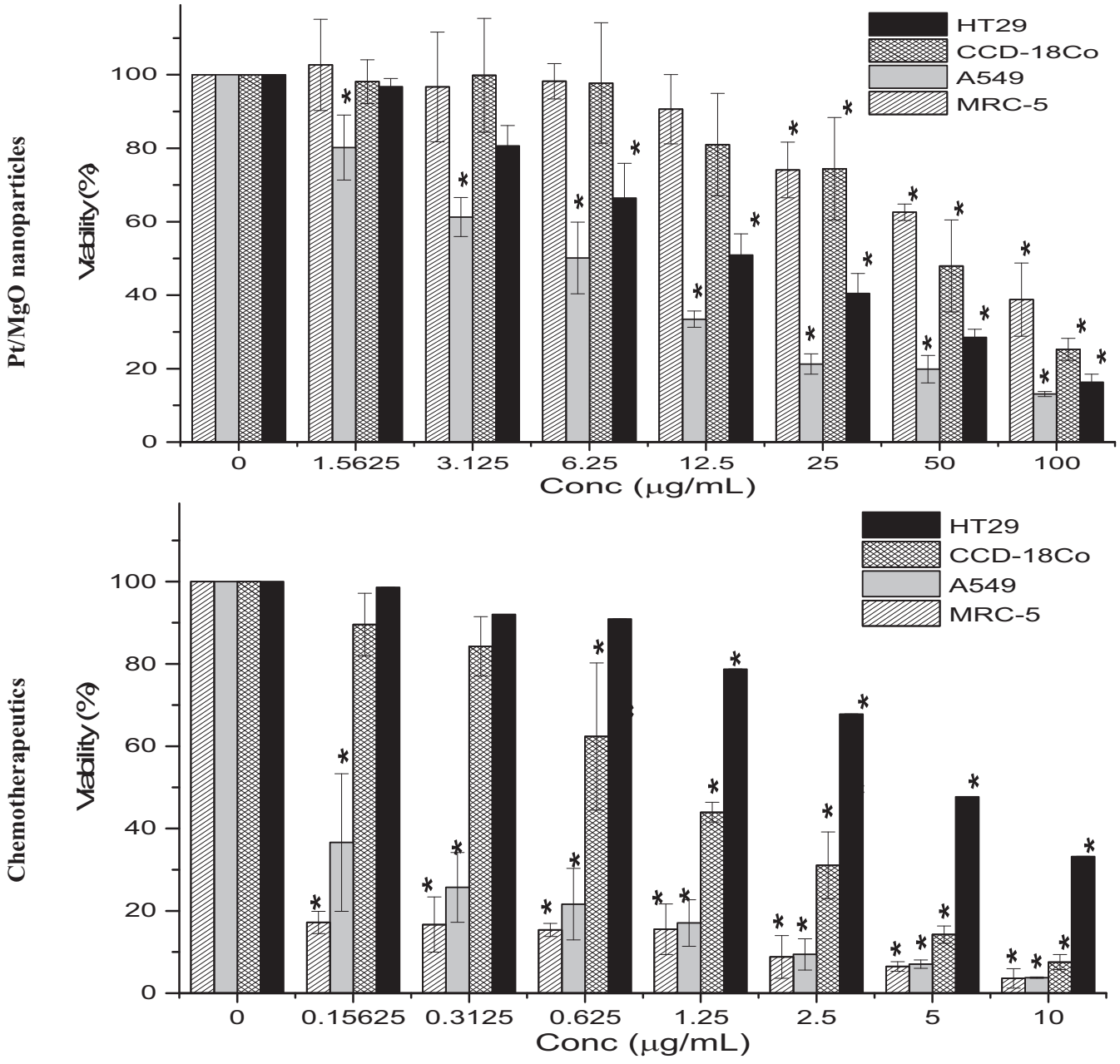

Fig. 3. Viability of cells treated with different concentrations of Pt/MgO nanoparticles and chemotherapeutics determined by the 3-(4,5-dimethylthiazol-2-yl)−2,5-diphenyltetrazolium bromide assay. The chemotherapeutic agents were oxaliplatin for human colorectal adenocarcinoma (HT29) and human normal colon (CCD-18Co) cell lines and paclitaxel for human lung carcinoma(A549) and normal human lung (MRC-5) cell lines. Values are mean ± standard deviation (n = 3 wells/treatment). *Means significantly different from non-treated cell means at $p < 0.05$.

Table 1
IC_{50} values of Pt/MgO nanoparticles, oxaliplatin, and paclitaxel on cancer and normal cell lines after 24 h treatment.

Cells	IC_{50} (μg/mL)		
	Pt/MgO	Oxaliplatin	Paclitaxel
CCD-18Co	48.08 ± 12.73	1.05 ± 0.81	–
MRC-5	76.83 ± 5.69	–	0.8 ± 1.6
HT29	13.65 ± 5.38	4.67 ± 0.03	–
A549	6.32 ± 9.44	–	0.12 ± 0.09

Note: HT29 = human colon adenocarcinoma cell line; CCD-18Co = human normal colon cell line; A549 = uman lung carcinoma cell line; MRC-5 = ormal human lung cell line.

sensitive to Pt/MgO nanoparticles than paclitaxel (Fig. 3). The MRC-5 cells were most resistant among cells to the growth inhibitory effect of paclitaxel, while the CCD-18Co cells were more sensitive to oxaliplatin than the HT29 cells (Fig. 3).

3.2.2. Caspase-3, -8 and -9

3.2.2.1. Caspase-3. The caspase-3 activities were significantly ($p < 0.05$) higher in treated than nontreated cancer cells. The HT29 andA549 cells, after treatment with 12.5 μg/mL Pt/MgO nanoparticles for 24 h, showed peak caspase-3 activities at736 and 599% higher than non-treated normal cells, respectively (Fig. 4). The same Pt/MgO nanoparticle concentration increased the caspase activities of CCD-18Co and MRC-5 cells by144 and 181% higher than non-treated control cells, at 12 and 24 h of treatment, respectively. The caspase-3 activities were effectively inhibited by the NAC pretreatment.

3.2.2.2. Caspase-8. The Pt/MgO nanoparticles activated cancer cell caspase-8 in a concentration-dependent manner (Fig. 4). The activities of caspase-8 in the A549 cell line after 12- and 24-hour treatment with 12.5 μg/mL Pt/MgO nanoparticles were 3.9- and 6.5-fold higher than in non-treated cells, respectively (Fig. 4). At the same concentration, the

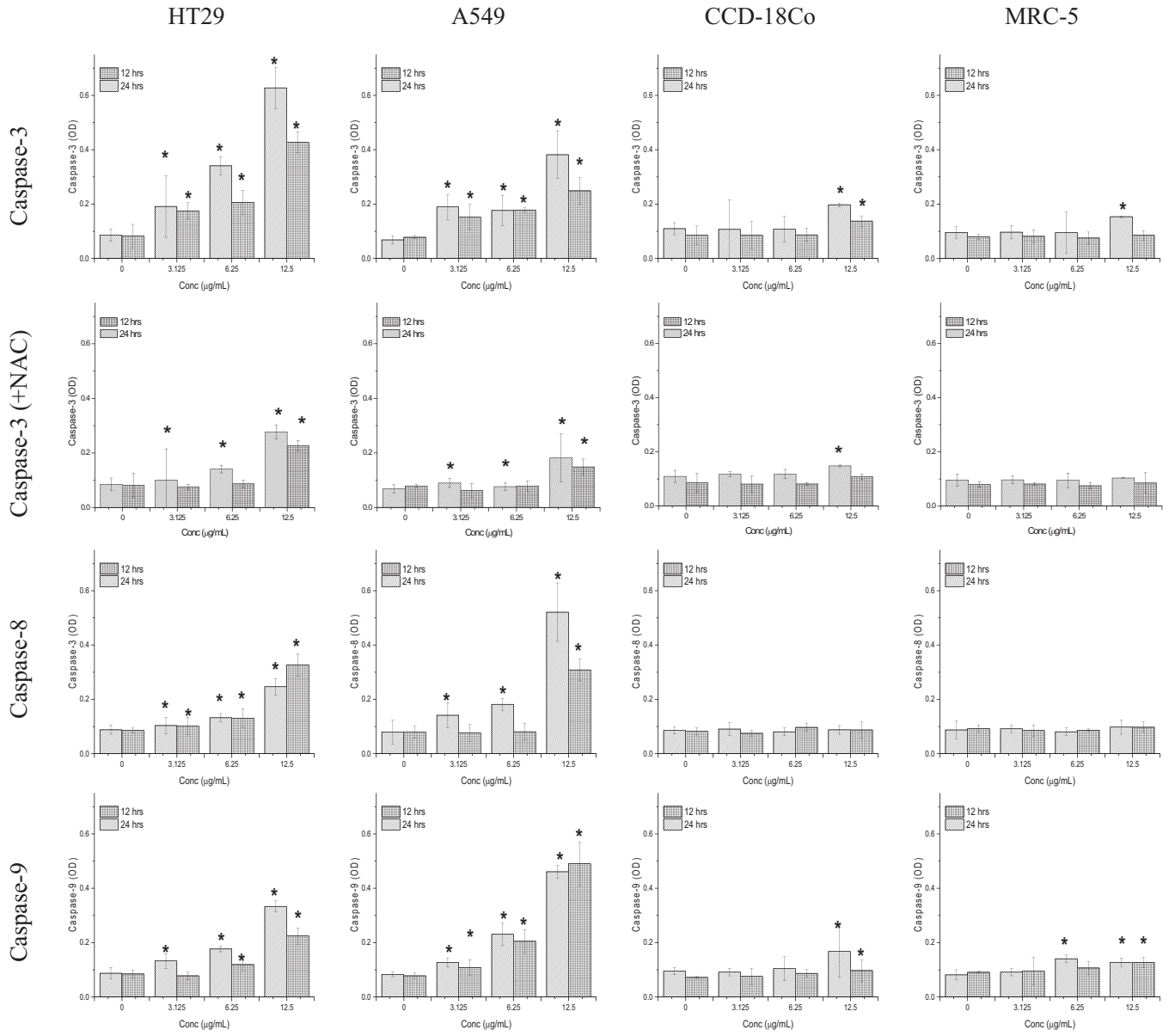

Fig. 4. Caspase-3, -8 and -9 activities inhuman colorectal adenocarcinoma (HT29), human lung carcinoma (A549), normal human colon (CCD-18Co), and normal human lung (MRC-5) cell lines after 12- and 24-h treatment with Pt/MgO nanoparticles at 3.125, 6.25 and 12.5 μg/mL. Caspase-3 activities were examined with and without 3 mM N-acetyl-L-cysteine (NAC). Values are mean ± standard deviation (n = 3 well/treatment). *Means significantly different from non-treated cell means at $p < 0.05$.

effect of Pt/MgO nanoparticles on caspase-8 activity was greater in A549 than HT29 cells. At lower concentrations of 3.125 and 6.25 μg/mL, Pt/MgO nanoparticles cause small increases in HT29 caspase-8 activities after 24 h of treatment. The caspase-8 activity of normal cells was not affected by treatment with Pt/MgO nanoparticles.

3.2.2.3. Caspase-9. The activity of caspase-9 in the colon cancer HT29 cell line increased significantly ($p < 0.05$) by 2.6- and 3.8-fold higher than non-treated control cells, after 12- and 24-h treatment with 12.5 μg/mL Pt/MgO nanoparticles, respectively (Fig. 4). The effect of Pt/MgO nanoparticles on HT29 cells was time- and concentration-dependent. No such increase in caspase-9 activity occurred in the A549 cells after 24 h treatment with 12.5 μg/mL Pt/MgO nanoparticles. Treatment with 6.25 μg/mL Pt/MgO nanoparticles for 12 and 24 h, markedly increased caspase-9 activities in HT29 cells by 141% and 202%, respectively, and in A549 cells by 262% and 278%, respectively, above the values for non-treated cells (Fig. 4). With 12.5 μg/mL Pt/MgO treatment, normal cells showed increases in caspase-9 activity beginning at 12 h and reaching a high value at24h.

3.2.3. Bcl-2, Bax, p53, and cytochrome C proteins

3.2.3.1. Bcl-2. The Bcl-2 protein level in A549 cells after 12-h treatment with 12.5 μg/mL Pt/MgO nanoparticles was more than 70% lower than in non-treated cells (Fig. 5). The down-regulation of BcL-2 in HT29 cells was time-dependent. In MRC-5 cells, significant 25% down-regulation($p < 0.05$) of Bcl-2 protein from non-treated cell values occurred after 24-h treatment with 12.5 μg/mL.Pt/MgO nanoparticles. Treatment with 12.5 μg/mL. Pt/MgO nanoparticles did not significantly ($p > 0.05$) affect Bcl-2 protein level in CCD-18Co cells.

3.2.3.2. Bax. Bax protein levels in A549 and HT29 cells treated with 12.5 μg/mL Pt/MgO nanoparticles were 2- to 4-fold higher than in non-treated cells (Fig. 5). The effect of Pt/MgO nanoparticles on the HT29 cells Bax protein level was concentration- and time-dependent. Pt/MgO nanoparticles treatment also increased the Bax protein levels in CCD-

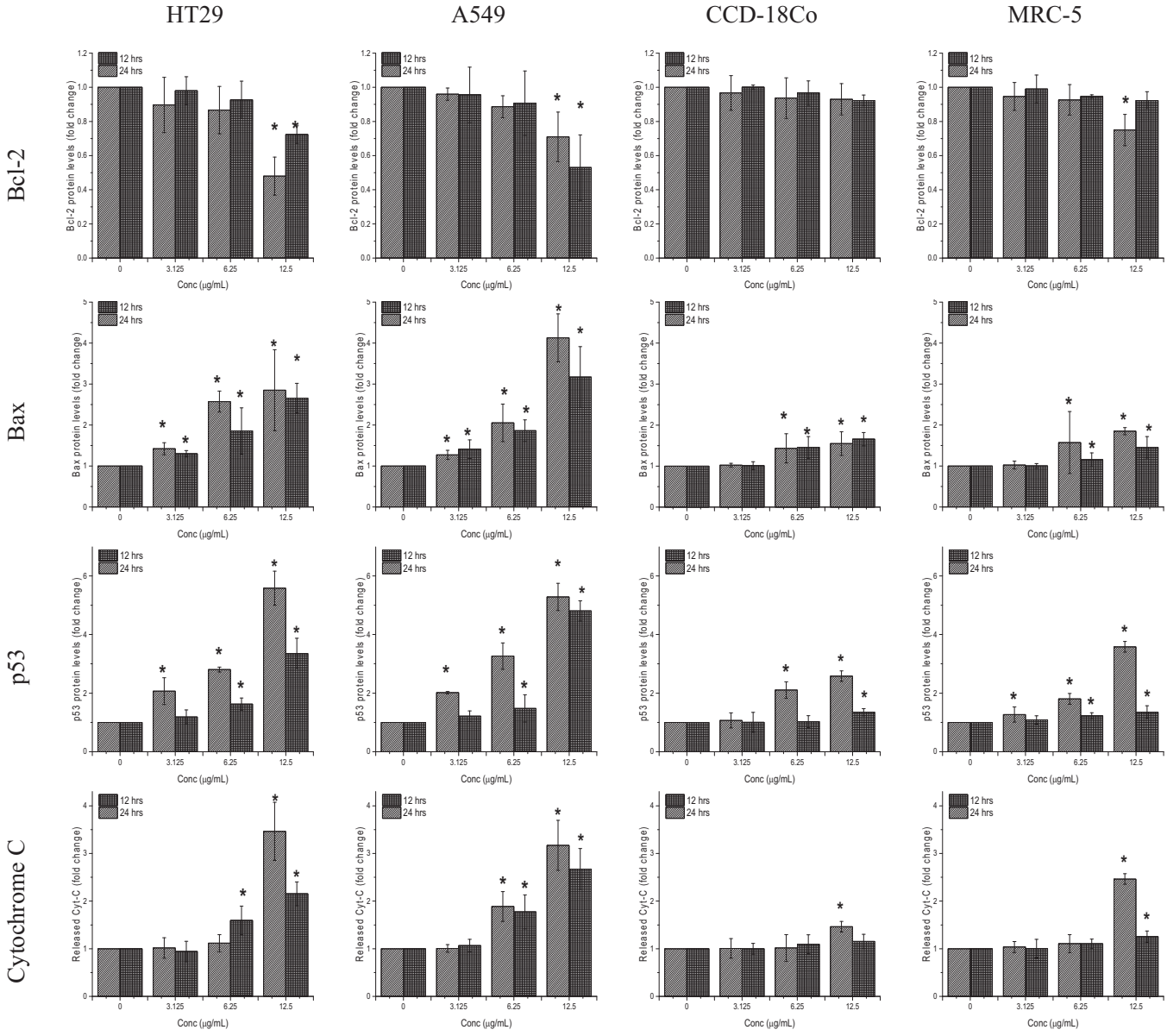

Fig. 5. Bcl-2, Bax, andp53 protein levels and cytochrome C release in human colorectal adenocarcinoma (HT29), human lung carcinoma (A549), normal human colon (CCD-18Co) and normal human lung (MRC-5) cells lines after 12- and 24-h treatment with Pt/MgO nanoparticles at 3.125, 6.25 and 12.5 μg/mL. Values are mean ± standard deviation (n = 3 well/treatment). *Means significantly different from non-treated cell means at $p < 0.05$.

19Co and MRC-5cells, although these increases were not as marked as in the HT29 and A549 cells.

3.2.3.3. p53. The p53 protein levels in HT29 and A549 cells increased significantly ($p < 0.05$) with increase in Pt/MgO nanoparticle treatment concentration. 12.5 μg/mL PtMgO nanoparticles caused increase in p53 levels in all cells used in the study. However, the effect of nanoparticle was more significant ($p < 0.05$) in the HT29 and A549 than CCD-18Co or MRC-5 cells (Fig. 5). However, in CCD-18Co cells, 12.5 μg/mL Pt/MgO nanoparticles significantly ($p < 0.05$) increased the p53 protein levels after 12-h treatment.

3.2.3.4. Cytochrome C. Cytochrome C releases by the HT29 and A549 cells were higher than by CCD-18Co and MRC-5 cells after treatment with 12.5 μg/mL Pt/Mg nanoparticles for24 than 12 h (Fig. 5). Pt/MgO nanoparticle treatment, at 3.125 and 6.25 μg/mL, did not affect cytochrome C release by the normal CCD-18Co and MRC-5 cells.

3.2.4. MDA, ROS, GSH and MPP

3.2.4.1. GSH. The effect of Pt/MgO nanoparticles on cellular anti-antioxidant mechanisms was determined by the changes in glutathione concentration in normal and cancer cells. In HT29, A549, CCD-18Co and MRC-5 cells treated with 12.5 μg/mL Pt/MgO nanoparticles for 24 h, there were decreases in glutathione concentration by approximately 39.1%, 61.7%, 5.1%, and 23.3%, respectively, in comparison to that of the non-untreated cells (Fig. 6).

3.2.4.2. MDA. Lipid peroxidation is a good indicator of oxidative stress in cells. The effects of Pt/MgO nanoparticles on cancer and normal cell lipid peroxidation are shown in Fig. 6. Treatment with 12.5 μg/mL Pt/MgO nanoparticles for 24 h increased the malondialdehyde concentrations of HT29, A549, CCD-18Co, and MRC-5 cells by 784%, 930%, 189%, and 494%, respectively, above that of the non-treated cells.

3.2.4.3. ROS. Treatment with 12.5 μg/mL Pt/MgO nanoparticles for 24 h increased A549 and HT29 cell ROS generation by approximately 3.6- and 2.8-fold higher than in non-treated cells, respectively (Fig. 6). The generation of ROS by similarly treated the normal MRC-5 was 162% higher than by the normal CCD-18Co cells.

3.2.4.4. Mitochondrial membrane potential assay M. We elucidated the effect of 12.5 μg/mL Pt/MgO nanoparticles on mitochondrial membrane potential using rhodamine 123 efflux. At 24 h, the percentage of cells with rhodamine 123 efflux was significantly lower ($p < 0.05$) in non-treated than treated cells. The highest rhodamine retention (40.5%) occurred in the A549 cells treated with 12.5 μg/mL Pt/MgO nanoparticles (Fig. 6). In fact, Pt/MgO nanoparticles were more effective at increasing rhodamine 123 efflux in cancer than normal cells.

3.2.5. Morphological examination

The morphology of cells treated with IC_{50} concentrations of Pt/MgO nanoparticles is shown in Fig. 7. After 24 h, non-treated cells were uniformly distributed in the culture plates and formed nearly complete monolayers. These cells were either round or oblong suggesting that they were intact. However, the HT29 and A549 cells treated with Pt/MgO nanoparticles showed loss of membrane integrity, shrinkage, membrane blebbing, and apoptosis. The effects of Pt/MgO nanoparticles were more severe on the HT29 than A549 cells. Pt/MgO nanoparticles-treated CCD-18Co and MRC-5 cells showed morphological evidences of deteriorating and dead cells.

4. Discussion

The co-precipitation method for aqueous solution is a promising approach in the synthesis of Pt/MgO nanoparticles. When sufficient amount of Pt is dissolved in excess MgO and rapidly heated, there is immediate reduction of the metal to form Pt/MgO nanoparticles. In the presence of excess MgO, metal nanoparticles serving as active sites, rapidly grow in the complexation with Pt. In the thermogravimetric analysis, the sizes of nanoparticles can be controlled by changing the heating process.

The results show that the Pt/MgO nanoparticles were pure. The purity of Pt/MgO nanoparticle suspensions is of utmost importance to eliminate side reactions from the presence of impurities. The purity of nanoparticles is essential if they are meant to be used as therapeutic compounds [24].

The Pt/MgO nanoparticles were unstable, have low electrostatic repulsion properties, and tend to aggregate in deionized and double-distilled water. However, the aggregation can be minimized by coating of the Pt/MgO nanoparticles with biocompatible polymers or conjugating with ligands that increases inter-particle distance [25], decreases the tendency of particle aggregation, and improve their potential to be developed as a therapeutic compound [26].

Transition metal-containing nanoparticles are now touted as the future in the treatment of diseases. These nanoparticles have fewer side effects and are cheaper to produce than current chemotherapeutic compounds [27]. Transition metal-containing nanoparticles bind to DNA, a property that can be benefited in the development of metal-based anti-cancer therapeutics [28]. For example, cisplatin, a platinum-containing anticancer drug, can interact with DNA through intra-strand cross-linkage and induce cell death. Unfortunately, cisplatin and its derivatives have serious side effects, including rapid development of drug resistance and cytotoxicity. Cisplatin is still not effective enough in the treatment of certain cancers like lung, colorectal, and prostate cancers [29,30]. Ruthenium compounds were used to form

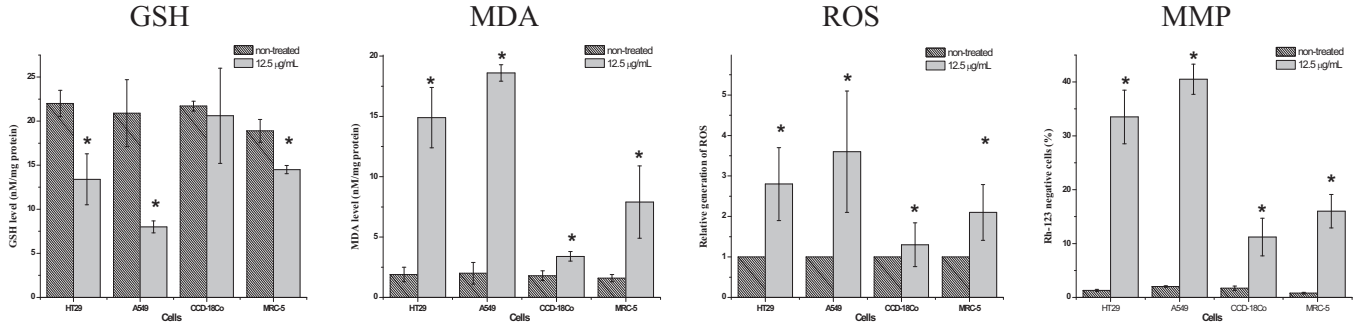

Fig. 6. Glutathione (GSH), malondialdehyde (MDA), and reactive oxygen species (ROS) concentrations, and mitochondrial transmembrane potential (MMP) of human colorectal adenocarcinoma (HT29), human lung carcinoma (A549), normal human colon (CCD-18Co) and normal human lung (MRC-5) cells lines after 24-h treatment with Pt/MgO nanoparticles at 12.5 μg/mL. Values are mean ± standard deviation (n = 3 well/treatment). *Means significantly different from non-treated cell means at $p < 0.05$.

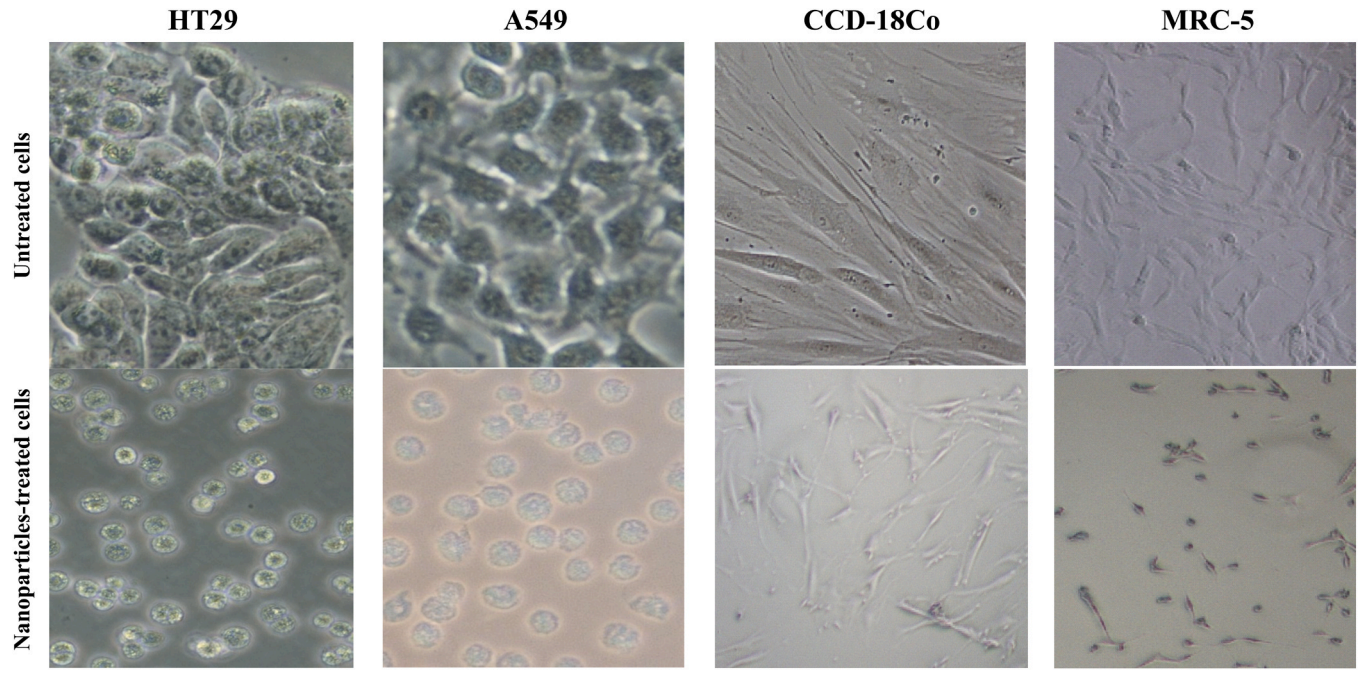

Fig. 7. Morphology of human colorectal adenocarcinoma (HT29), human lung carcinoma (A549), normal human colon (CCD-18Co) and normal human lung (MRC-5) cells lines treated with Pt/MgO nanoparticles at IC_{50} concentration. (200×).

complexes with cisplatin, as a mean to overcome the deficiencies in the anti-cancer effects of the therapeutic compound [31,32].

The dose and treatment periods for Pt/MgO nanoparticles elected for the study were based on our recent published work [33]. The safety of Pt/MgO nanoparticles as a potential therapeutic agent was determined on the normal colon, CCD-18Co and lung, MRC-5, cells. Pt/MgO nanoparticles did not adversely affect the viability of these cells. However, the nanoparticles, even at low concentrations of 3.125 and 6.25 μg/mL, were toxic to the HT29 and A549 cell lines.

The cancer cell microenvironment is acidic [34–36]. Incidentally, MgO dissociates at acidic pH [37] allowing for easy release of Pt from the Pt/MgO complex in the cancer tissues. This property of Pt/MgO nanoparticles offers an improved strategy in the treatment of cancers.

Oxidative stress is the result of imbalance between oxidants and antioxidants and reactive oxygen species (ROS) in the cellular environments [38]. The generation of ROS, particularly the reactive hydroxyl radicals, induces lipid peroxidation [39] that can damage the phospholipids of membrane bilayer, causing loss of membrane integrity [39,40]. Evidently, Pt/MgO nanoparticles increased ROS generation and lipid peroxidation in the HT29 and A549 cells, which is presumed to contribute to anti-cancer effects of the nanoparticles. Platinum-containing drugs induce oxidative stress by increasing ROS [41] and decreasing glutathione production [42], which will culminate in the induction of apoptosis via the p53, survivin, Bax/Bcl-2, and caspase pathways. Glutathione is the endogenous antioxidant that protects cells from oxidative stress by serving as a substrate for enzymatic antioxidants [43]. In the current study, cancer cells had low glutathione levels after treatment with Pt/MgO nanoparticles for 24 h. This resulted in the failure of cancer cells to effectively eliminate ROS, hydrogen peroxide, and metabolites, compromising cellular antioxidant defenses, resulting in damage and eventually death of these cells [44–46].

Caspase-9 and -8 mediate intracellular cell-death signaling via the intrinsic mitochondria-mediated and extrinsic death receptor-mediated apoptotic pathways, respectively [47,48]. Caspase-3 serves as the down-stream enzyme that mediates both pathways for eventual apoptosis. The study showed that treatment with Pt/MgO nanoparticles activated the apoptotic pathways in the HT29 and A549 cells. Pre-treatment with NAC, the GSH precursor, may abrogate the Pt/MgO nanoparticle-induced caspase-3activities in the cancer cells and inhibiting apoptosis.

Our study showed increased mitochondrial membrane permeability in cancer cells treated with Pt/MgO nanoparticles, with concurrent decrease in Bcl-2 and increase in Bax and p53 levels. These findings suggest that Pt/MgO induced cancer cell apoptosis through the down-regulation of anti-apoptotic protein, Bcl-2 and up-regulation of pro-apoptotic Bax and p53, culminating in mitochondrial membrane depolarization, release of cytochrome C, and activation of the apoptotic pathways. Clearly, the apoptotic effects of Pt/MgO nanoparticles on cancer cells were via both the intrinsic and the extrinsic pathways. The Pt/MgO nanoparticles also exert anti-cancer activities by up-regulating the anti-tumor suppressor, p53, protein.

5. Conclusion

Pt/MgO nanoparticles were cuboid in structure with the size range of 30–50 nm. Treatment of cancer cells with Pt/MgO nanoparticles significantly increased their ROS and lipid peroxidation activities and decreased glutathione concentration. Pt/MgO nanoparticles also inhibited proliferation of lung and colonic cancer cells through the activation of the intrinsic and extrinsic apoptotic pathways. This was evident by the increase in the caspase-3, -9, and -8 activities, down-regulation of Bcl-2 and up-regulation of Bax proteins in cancer cells. The Pt/MgO nanoparticles-induced apoptosis was inhibited by NAC pretreatment, indicating that the anti-cancer effects of Pt/MgO are partly through the inhibition of oxidative stress. In conclusion, Pt/MgO nanoparticles are selectively toxic to colon and lung cancer cells and have great potential to be developed as an anti-cancer therapeutic compound.

Acknowledgement

The publication of this article was funded by the Qatar National Library.

References

[1] M.S. Al-Qubaisi, A. Rasedee, M.H. Flaifel, S.H. Ahmad, S. Hussein-Al-Ali, M. Z. Hussein, Z. Zainal, F.H. Alhassan, Y.H. Taufiq-Yap, E.E. Eid, Induction of apoptosis in cancer cells by NiZn ferrite nanoparticles through mitochondrial cytochrome C release, Int. J. Nanomed. 8 (2013) 4115.

[2] M.S. Al-Qubaisi, A. Rasedee, M.H. Flaifel, S.H. Ahmad, S. Hussein-Al-Ali, M. Z. Hussein, E.E. Eid, Z. Zainal, M. Saeed, M. Ilowefah, Cytotoxicity of nickel zinc ferrite nanoparticles on cancer cells of epithelial origin, Int. J. Nanomed. 8 (2013) 2497.

[3] J. Kavanagh, Sodium, potassium, calcium, magnesium, zinc, citrate and chloride content of human prostatic and seminal fluid, J. Reprod. Fertil. 75 (1) (1985) 35–41.

[4] J.F. Da Silva, R.J.P. Williams, The Biological Chemistry of the Elements: The Inorganic Chemistry of Life, Oxford University Press, 2001.

[5] C. Suelter, Monovalent cations in enzyme-catalyzed reactions, Met. Ions Biol. Syst. 3 (1974) 201–251.

[6] C. Bai, M. Tang, Toxicological study of metal and metal oxide nanoparticles in zebrafish, J. Appl. Toxicol. 40 (1) (2020) 37–63.

[7] B. Zhu, K. Qiu, C. Shang, Z. Guo, Naturally derived porous carbon with selective metal-and/or nitrogen-doping for efficient CO 2 capture and oxygen reduction, J. Mater. Chem. A 3 (9) (2015) 5212–5222.

[8] C.G. Fraga, Relevance, essentiality and toxicity of trace elements in human health, Mol. Asp. Med. 26 (4–5) (2005) 235–244.

[9] W. Yang, P.J. Weng, Y. Gao, A new paradigm of DNA synthesis: three-metal-ion catalysis, Cell Biosci. 6 (1) (2016) 51.

[10] A. Le Goff, V. Artero, B. Jousselme, P.D. Tran, N. Guillet, R. Métayé, A. Fihri, S. Palacin, M. Fontecave, From hydrogenases to noble metal–free catalytic nanomaterials for H2 production and uptake, Science 326 (5958) (2009) 1384–1387.

[11] P.K. Jain, X. Huang, I.H. El-Sayed, M.A. El-Sayed, Noble metals on the nanoscale: optical and photothermal properties and some applications in imaging, sensing, biology, and medicine, Acc. Chem. Res. 41 (12) (2008) 1578–1586.

[12] J. Virkutyte, R.S. Varma, Green synthesis of metal nanoparticles: biodegradable polymers and enzymes in stabilization and surface functionalization, Chem. Sci. 2 (5) (2011) 837–846.

[13] E. Ahmadian, A. Eftekhari, H. Babaei, A.M. Nayebi, M.A. Eghbal, Anti-cancer effects of citalopram on hepatocellular carcinoma cells occur via cytochrome C release and the activation of NF-kB, Anti-Cancer Agents Med. Chem. (Former. Curr. Med. Chem. -Anti-Cancer Agents) 17 (11) (2017) 1570–1577.

[14] M. Al-Fahdawi, A. Rasedee, M. Al-Qubaisi, Cytotoxicity and physicochemical characterization of iron–manganese-doped sulfated zirconia nanoparticles [Corrigendum], Int. J. Nanomed. 10 (2015) 6657.

[15] J.J. Li, D. Hartono, C.-N. Ong, B.-H. Bay, L.-Y.L. Yung, Autophagy and oxidative stress associated with gold nanoparticles, Biomaterials 31 (23) (2010) 5996–6003.

[16] H.J. Groot, F.E. van Leeuwen, S. Lubberts, S. Horenblas, R. de Wit, J.A. Witjes, G. Groenewegen, P.M. Poortmans, M.C. Hulshof, O.W. Meijer, Platinum exposure and cause-specific mortality among patients with testicular cancer, Cancer 126 (3) (2020) 628–639.

[17] E. Birben, U.M. Sahiner, C. Sackesen, S. Erzurum, O. Kalayci, Oxidative stress and antioxidant defense, World Allergy Organ. J. 5 (1) (2012) 9–19.

[18] D.J. Betteridge, What is oxidative stress? Metabolism 49 (2) (2000) 3–8.

[19] M.M. Gaschler, B.R. Stockwell, Lipid peroxidation in cell death, Biochem. Biophys. Res. Commun. 482 (3) (2017) 419–425.

[20] A. Borowik, R. Banasiuk, N. Derewonko, M. Rychlowski, M. Krychowiak-Masnicka, D. Wyrzykowski, M. Ziabka, A. Woziwodzka, A. Krolicka, J. Piosik, Interactions of newly synthesized platinum nanoparticles with ICR-191 and their potential application, Sci. Rep. 9 (1) (2019) 1–11.

[21] A. Sharma, A.K. Goyal, G. Rath, Recent advances in metal nanoparticles in cancer therapy, J. Drug Target. 26 (8) (2018) 617–632.

[22] F.J. Al-Doghachi, Z. Zainal, M.I. Saiman, Z. Embong, Y.H. Taufiq-Yap, Hydrogen production from dry-reforming of biogas over Pt/Mg1-xNixO catalysts, Energy Procedia 79 (2015) 18–25.

[23] R.R. Devi, I.M. Umlong, P.K. Raul, B. Das, S. Banerjee, L. Singh, Defluoridation of water using nano-magnesium oxide, J. Exp. Nanosci. 9 (5) (2014) 512–524.

[24] C. Sun, L. Wen, J. Zeng, Y. Wang, Q. Sun, L. Deng, C. Zhao, Z. Li, One-pot solventless preparation of PEGylated black phosphorus nanoparticles for photoacoustic imaging and photothermal therapy of cancer, Biomaterials 91 (2016) 81–89.

[25] M. Zahraei, M. Marciello, A. Lazaro-Carrillo, A. Villanueva, F. Herranz, M. Talelli, R. Costo, A. Monshi, D. Shahbazi-Gahrouei, M. Amirnasr, Versatile theranostics agents designed by coating ferrite nanoparticles with biocompatible polymers, Nanotechnology 27 (25) (2016), 255702.

[26] R.K. Keservani, A.K. Sharma, Nanoparticulate Drug Delivery Systems, Apple Academic Press, 2019.

[27] N. Muhammad, Z. Guo, Metal-based anticancer chemotherapeutic agents, Curr. Opin. Chem. Biol. 19 (2014) 144–153.

[28] M.S. Shoshan, T. Vonderach, B. Hattendorf, H. Wennemers, Peptide-coated platinum nanoparticles with selective toxicity against liver cancer cells, Angew. Chem. Int. Ed. 58 (15) (2019) 4901–4905.

[29] G.F. Nordberg, B.A. Fowler, M. Nordberg, Handbook on the Toxicology of Metals, Academic Press, 2014.

[30] Z. Liu, P.J. Sadler, Organoiridium complexes: anticancer agents and catalysts, Acc. Chem. Res. 47 (4) (2014) 1174–1185.

[31] A. D'Amora, M.E. Cucciolito, R. Iannitti, G. Morelli, R. Palumbo, F. Ruffo, D. Tesauro, Pyridine ruthenium (III) complexes entrapped in liposomes with enhanced cytotoxic properties in PC-3 prostate cancer cells, J. Drug Deliv. Sci. Technol. 51 (2019) 552–558.

[32] J.-Q. Wang, P.-Y. Zhang, L.-N. Ji, H. Chao, A ruthenium (II) complex inhibits tumor growth in vivo with fewer side-effects compared with cisplatin, J. Inorg. Biochem. 146 (2015) 89–96.

[33] M.Q. Al-Fahdawi, A. Rasedee, F.A. Al-Doghachi, R. Rosli, Y.H. Taufiq-Yap, M.S. Al-Qubaisi, Anticancer palladium-doped magnesia nanoparticles: synthesis, characterization, and in vitro study, Nanomedicine 15 (06) (2020) 547–561.

[34] M. Kundu, P. Sadhukhan, N. Ghosh, S. Chatterjee, P. Manna, J. Das, P.C. Sil, pH-responsive and targeted delivery of curcumin via phenylboronic acid-functionalized ZnO nanoparticles for breast cancer therapy, J. Adv. Res. 18 (2019) 161–172.

[35] M.S. Al-Qubaisi, A. Rasedee, M.H. Flaifel, E.E. Eid, S. Hussein-Al-Ali, F.H. Alhassan, A.M. Salih, M.Z. Hussein, Z. Zainal, D. Sani, Characterization of thymoquinone/hydroxypropyl-β-cyclodextrin inclusion complex: application to anti-allergy properties, Eur. J. Pharm. Sci. 133 (2019) 167–182.

[36] A.S. Al-Abboodi, E.E. Eid, F. Azam, M.S. Al-Qubaisi, Inclusion complex of clausenidin with hydroxypropyl-β-cyclodextrin: improved physicochemical properties and anti-colon cancer activity, Saudi Pharm. J. (2021).

[37] E. Soudée, J. Péra, Mechanism of setting reaction in magnesia-phosphate cements, Cem. Concr. Res. 30 (2) (2000) 315–321.

[38] M. Battino, P. Bullon, M. Wilson, H. Newman, Oxidative injury and inflammatory periodontal diseases: the challenge of anti-oxidants to free radicals and reactive oxygen species, Crit. Rev. Oral. Biol. Med. 10 (4) (1999) 458–476.

[39] A. Catalá, Lipid peroxidation of membrane phospholipids generates hydroxy-alkenals and oxidized phospholipids active in physiological and/or pathological conditions, Chem. Phys. Lipids 157 (1) (2009) 1–11.

[40] R.M. Cordeiro, Reactive oxygen species at phospholipid bilayers: distribution, mobility and permeation, Biochim. Biophys. Acta (BBA)-Biomembr. 1838 (1) (2014) 438–444.

[41] M. Aioub, S.R. Panikkanvalappil, M.A. El-Sayed, Platinum-coated gold nanorods: efficient reactive oxygen scavengers that prevent oxidative damage toward healthy, untreated cells during plasmonic photothermal therapy, ACS Nano 11 (1) (2017) 579–586.

[42] L. Nejdl, J. Kudr, A. Moulick, D. Hegerova, B. Ruttkay-Nedecky, J. Gumulec, K. Cihalova, K. Smerkova, S. Dostalova, S. Krizkova, Platinum nanoparticles induce damage to DNA and inhibit DNA replication, PLoS One 12 (7) (2017), e0180798.

[43] S.-i Usami, O.P. Hjelle, O.P. Ottersen, Differential cellular distribution of glutathione–an endogenous antioxidant–in the guinea pig inner ear, Brain Res. 743 (1–2) (1996) 337–340.

[44] M. Alía, R. Mateos, S. Ramos, E. Lecumberri, L. Bravo, L. Goya, Influence of quercetin and rutin on growth and antioxidant defense system of a human hepatoma cell line (HepG2), Eur. J. Nutr. 45 (1) (2006) 19–28.

[45] M. Iborra, I. Moret, F. Rausell, G. Bastida, M. Aguas, E. Cerrillo, P. Nos, B. Beltrán, Role of Oxidative Stress and Antioxidant Enzymes in Crohn's Disease, Portland Press Limited, 2011.

[46] A. Gizi, I. Papassotiriou, F. Apostolakou, C. Lazaropoulou, M. Papastamataki, I. Kanavaki, V. Kalotychou, E. Goussetis, A. Kattamis, I. Rombos, Assessment of oxidative stress in patients with sickle cell disease: the glutathione system and the oxidant–antioxidant status, Blood Cells, Mol. Dis. 46 (3) (2011) 220–225.

[47] M. Al-Qubaisi, R. Rozita, S.-K. Yeap, A.-R. Omar, A.-M. Ali, N.B. Alitheen, Selective cytotoxicity of goniothalamin against hepatoblastoma HepG2 cells, Molecules 16 (4) (2011) 2944–2959.

[48] M. Al-Qubaisi, R. Rosli, T. Subramani, A.R. Omar, S.K. Yeap, A.M. Ali, N. B. Alitheen, Goniothalamin selectively induces apoptosis on human hepatoblastoma cells through caspase-3 activation, Nat. Prod. Res. 27 (23) (2013) 2216–2218.